공학석사학위논문

Determination of Operational Limits for High-Altitude Long-Endurance Aircraft Considering Propeller Icing

프로펠러 결빙을 고려한 고고도 장기 체공 무인기의 운용 한계 결정

2023년 8월

서울대학교 대학원

항공우주공학과

박 지 민

Determination of Operational Limits for High-Altitude Long-Endurance Aircraft Considering Propeller Icing

프로펠러 결빙을 고려한 고고도 장기 체공 무인기의 운용 한계 결정

지도교수 이 관 중

이 논문을 공학석사 학위논문으로 제출함

2023년 8월

서울대학교 대학원

항공우주공학과

박 지 민

박지민의 공학석사 학위논문을 인준함

2023년 8월

위 원 장 김규홍 (인)

부위원장 이관중 (인)

위 원 손찬규 (인)

Abstract

High-Altitude Long-Endurance UAVs (HALE UAV) are being researched and developed by several research institutes and manufacturers around the world because they can perform various tasks such as providing broadcasting services, real-time disaster monitoring, and reconnaissance. However, icing may occur during the in-flight process of climbing and descending during the operation of a high-altitude long-term flight under icing conditions. This may cause damage because it is difficult to install the de-icing device due to its design characteristics.

Therefore, this study selects icing environments that the aircraft could encounter and simulates icing on the fuselage, wing, and propeller. Then a method to determine the operating limit area of the aircraft by calculating the total amount of energy required for operation through performance analysis of the changed shape is presented. In this process, the computational efficiency is increased by using two-dimensional analysis method (BEMT) for propeller icing simulation, and individual icing simulation of propeller and fuselage & wing parts. The results showed three parameters: analysis of ice shape and performance changes in the fuselage & wing, analysis of ice shape and performance changes in the propeller, and

confirmation that the icing on the propeller has a significant impact on determining the operating limitations of HALE UAV.

Keyword : High-Altitude Long-Endurance UAV(HALE UAV), Icing, Propeller, BEMT

Student Number : 2021-27606

Table of Contents

Abstract i

Chapter 1. Introduction 1

Chapter 2. Numerical methods 5

2.1. Problem definition 7

2.2. Icing simulation 7

2.2.1. Wing & fuselage icing simulation 7

2.2.2. Propeller icing simulation 7

2.3. Performance analysis 10

2.4. Determination of operation limit 13

Chapter 3. Validation of numerical methods 16

3.1. In−flight icing code validation 16

3.2. BEMT based 2D icing solver validation 16

Chapter 4. Problem definition 20

Chapter 5. Results & Discussions 23

5.1. Computational domain & Boundary conditions 23

5.2. Ice shape prediction and analysis 25

5.2.1. Icing results of wing & fuselage 25

5.2.2. Icing results of propeller 30

5.2.3. Operational limits analysis 32

Chapter 6. Conclusions 34

Bibliography 36

Abstract in Korean 38

Chapter 1. Introduction

High-altitude long-endurance (HALE) aircraft are unmanned aerial vehicles (UAVs) that operate in the stratosphere at altitudes exceeding 15 km for extended periods to conduct missions such as observation, monitoring, and communication relay. Due to their relatively lower acquisition and operational costs compared to satellites, HALE UAVs are being developed by several research agencies and aircraft manufacturers. However, in-flight icing during the climb stage of such aircraft can result in their failure to reach the desired mission altitude. This poses a significant challenge since the ultra-light design of HALE UAVs precludes the installation of de-icing equipment. Consequently, any ice that accumulates on the aircraft surface persists for prolonged periods, leading to degradation in aerodynamic performance by altering surface roughness and increasing total mass.

A few studies have analyzed the effect of icing on HALE UAVs. According to Vogel [1], icing on HALE aircraft is a significant environmental factor that can limit the operational capabilities of HALE aircraft. Vogel also found that the accumulation of ice on the wings of HALE aircraft can lead to a decrease in the rate of climb (ROC), which can have a significant impact on their operations.

Therefore, the importance of having ice-detecting equipment during HALE aircraft operation was emphasized to ensure safety. In the study conducted by Iya and Cook [2], the prediction of the shape of ice formation on the airfoil of HALE aircraft wings was investigated. Iya also calculated the time required for the accumulated ice to sublimate. Bottyan [3] conducted a study on the prediction of the shape of ice formation on a cylinder with the same radius as the airfoil of a HALE wing. Bottyan also confirmed the performance degradation caused by ice formation on the cylinder and found that the performance degradation becomes more severe as the ice shape changes from rime to glaze. Son [4] identified potential icing conditions that HALE UAVs could encounter during in-flight operations and predicted the resulting ice shapes. Then, he evaluated the performance changes and determined the operational limits based on the required battery capacity ratio relative to the given battery capacity.

Previous studies on the effects of icing on HALE UAVs have mainly focused on the icing effects on the fuselage, neglecting the influence on the propellers. However, the propeller sections have relatively short chord length and large inflow velocity, which can result in more severe shape changes and greater susceptibility to icing. In addition, if the efficiency of the propeller decreases due to

icing, a higher RPM may be required to achieve the desired performance, which can affect the efficiency of the motor connected to the propeller. Therefore, it is essential to consider propeller icing when analyzing the effects of icing on HALE UAVs.

However, addressing this concern presents challenges. The process of establishing operational limitations for HALE aircraft demands an extensive number of 3D CFD analyses. Predicting icing across various conditions necessitates accounting for icing on stationary components such as wings and fuselage, as well as on the rotating propeller. Consequently, this undertaking incurs substantial computational costs.

Taking these factors into consideration, the objective of this study is to determine the operational limits of a HALE UAV by accounting for propeller icing effects.

To achieve this goal, 3D icing simulations for the fuselage and wing sections, excluding the propeller, are performed. Also, the 2D icing simulations using a Blade Element Momentum Theory (BEMT) based approach are performed for the propeller. These simulation methods are validated by comparing them with experimental results. Independent icing simulations are performed for the propeller and the fuselage-wing sections, excluding the propeller. In reality, interactions would occur between the propeller and the downstream

fuselage & wing sections. However, in this study, an independent icing simulation was conducted by applying the assumption that the propeller's icing has less effect on the fuselage & wing because the propeller's radius is about 12% smaller than the span of the wing.

Finally, in the process of determining the operational limits, the Kriging method is applied to handle a wide range of icing conditions. The use of Kriging allowed the increase in computational efficiency, as it requires a relatively small number of sampling points. This approach enabled us to comprehensively address a broad icing environment.

Chapter 2. Methodology

To determine the operational limits, the procedure consists of four main stages, namely problem definition, icing simulation, performance analysis, and determination of operational limit, as depicted in the Fig. 1.

2.1. Problem definition

In the first stage, which is the problem definition phase, aircraft model selection, icing condition selection, icing exposure time decision, and determination of icing exposure time are conducted. The currently under-research and development aircraft model has been chosen, and in accordance with the regulations and directives of the Federal Aviation Regulations(FARs) that outline parameters affecting icing, nine icing environments are identified, Additionally, based on the mission profile of the selected aircraft and the icing environment, the distance exposed to icing is divided by the aircraft's cruising speed to determine the exposure time to icing in the icing environment.

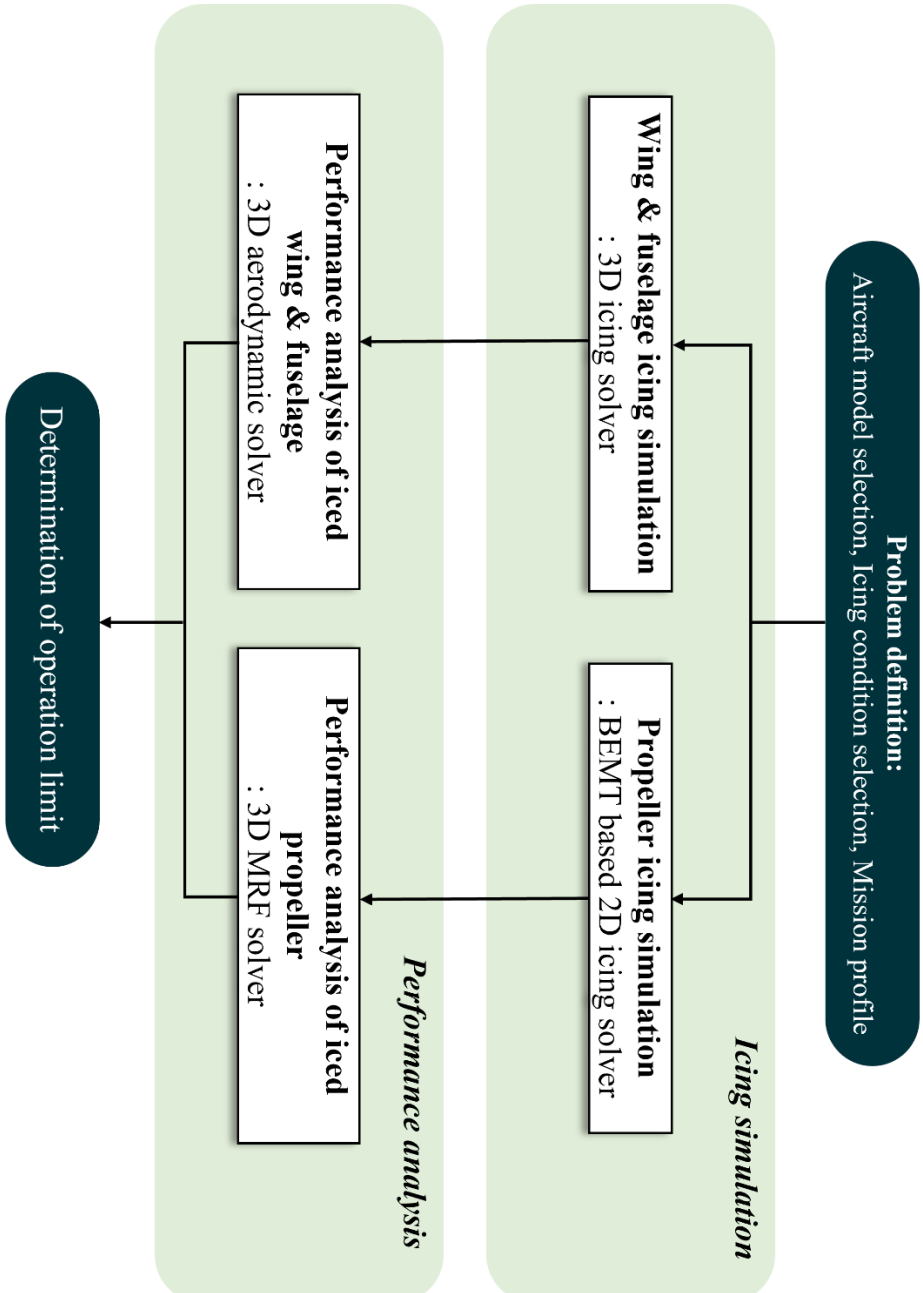

Fig. 1 Basic structure for determining operation limit

2.2. Icing simulation

2.2.1. Wing & fuselage icing simulation

This study utilized ICEPAC, an icing analysis solver developed by Son [5], which is based on the open-source computational fluid dynamics software OpenFOAM [6]. ICEPAC consists of four modules: 1) aerodynamic, 2) droplet field, 3) thermodynamic, and 4) ice growth modules. Each module applies the quasi-steady assumption, and the results from each module are used sequentially as inputs for the following module. In the aerodynamic module, the compressible Reynolds-averaged Navier-Stokes equations are solved using the rhoPimpleFoam solver in OpenFOAM. The droplets field module employs the Eulerian approach and considers drag, gravity, and buoyancy forces acting on the droplets. The Shallow Water Icing Model [7] is used in the thermodynamic module to solve the mass and energy conservation of the water film., Finally, in the ice growth module, the mass of accumulated ice is calculated, and the resulting ice thickness is determined.

2.2.2. Propeller icing simulation

To analyze propeller icing efficiently, a two-dimensional approach was used due to the high computational resources required for three-dimensional simulations. In this method, the propeller

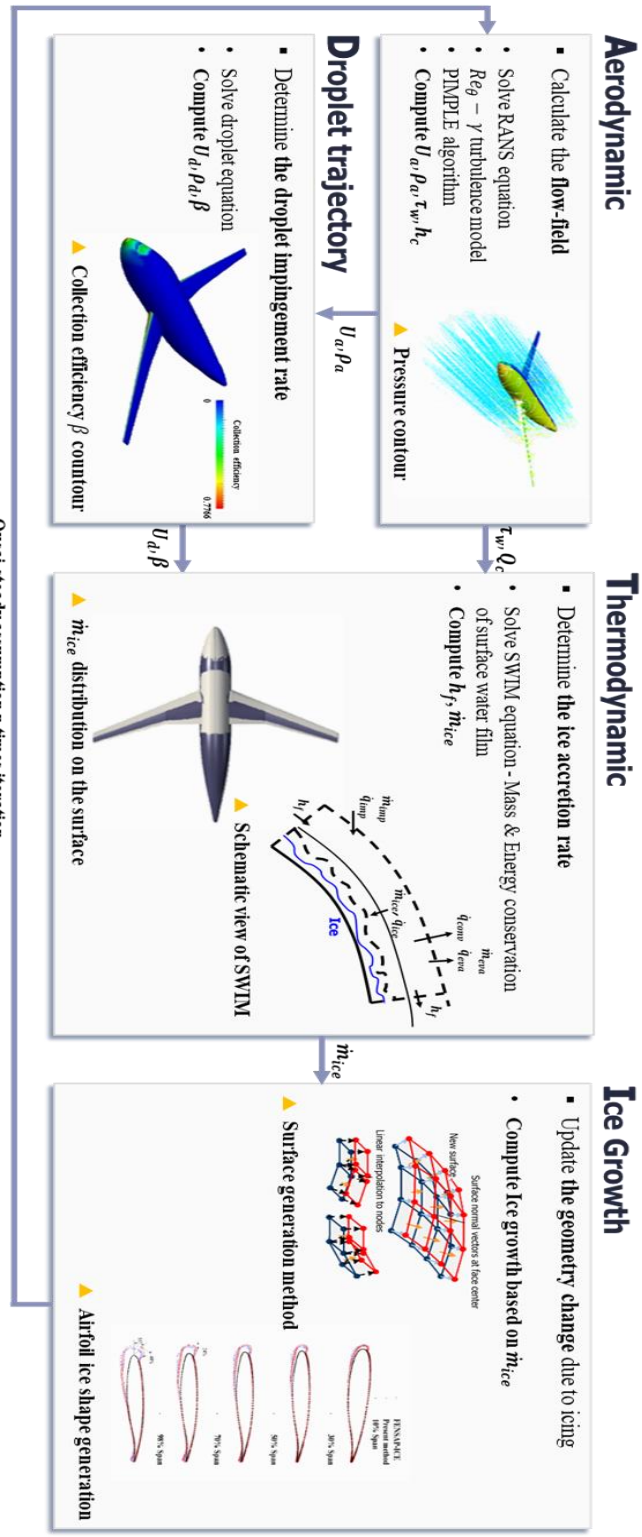

Fig. 2 Structure of the basic icing solver ICEPAC [5]

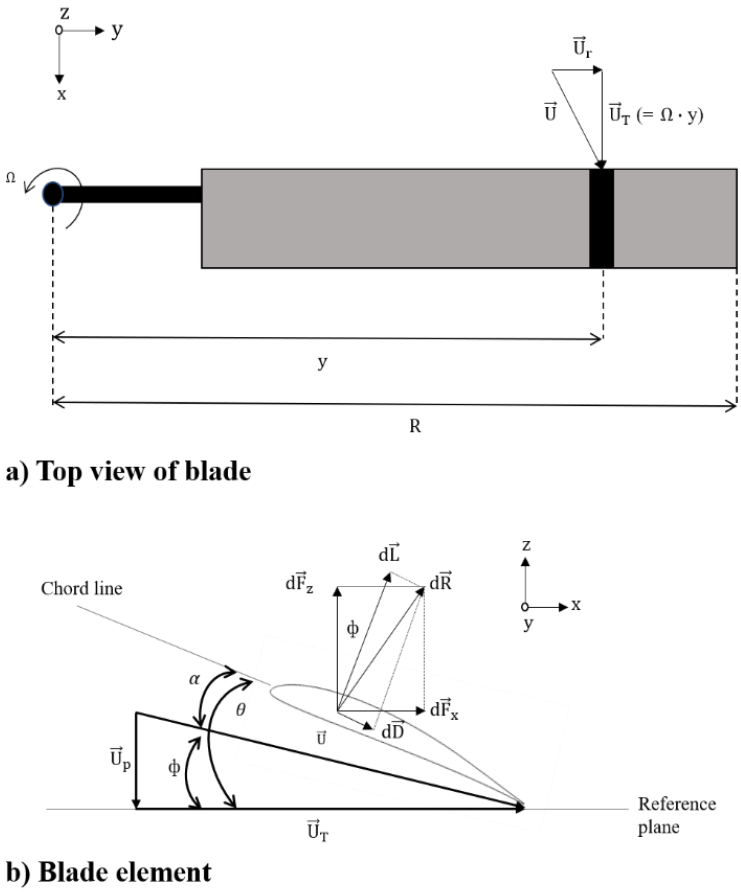

Fig. 3 Flow environments at the blade element [8]

blade is divided into multiple two-dimensional sections along the span direction. Then, the Blade Element Momentum Theory (BEMT) and the ICPEAC is combined to predict the ice shapes on each section. The input conditions for ICEPAC are calculated using the BEMT. Fig. 3 illustrates the forces acting on the blade element in the surrounding environment. The inflow ratio is then calculated using Prandtl's tip loss factor as shown in Equation 1.

$$\lambda(r) = \frac{\sigma \cdot C_{L_\alpha}}{16F} \cdot \left(\sqrt{1 + \frac{32F}{\sigma \cdot C_{L_\alpha}} \theta(r) \cdot r} - 1 \right) \tag{1}$$

The input conditions that have been determined are utilized to predict the icing shapes, as depicted in Fig 4. The icing shapes are predicted for each section, and then the changed shapes caused by icing are used to repeat the process.

Next, the effective angle of attack and induced inflow velocity are determined by correlating the inflow angle and inflow ratio using Equation 2 to 4.

$$\phi(r) = \frac{\lambda(r)}{r} \tag{2}$$

$$\vec{u}_p(r) = \vec{u}_p(r) \cdot \phi(r) \tag{3}$$

$$\alpha(r) = \theta(r) - \phi(r) \tag{4}$$

2.3. Performance analysis

Performance analysis is conducted separately for the wing−body section and the propeller as depicted in Fig 5. Firstly, for the wing−body section, full 3D CFD simulation is employed to predict the icing shape. Grid remeshing is performed using the newly generated 3D grid, and performance analysis is carried out, considering lift coefficient, drag coefficient, and mass flow rate.

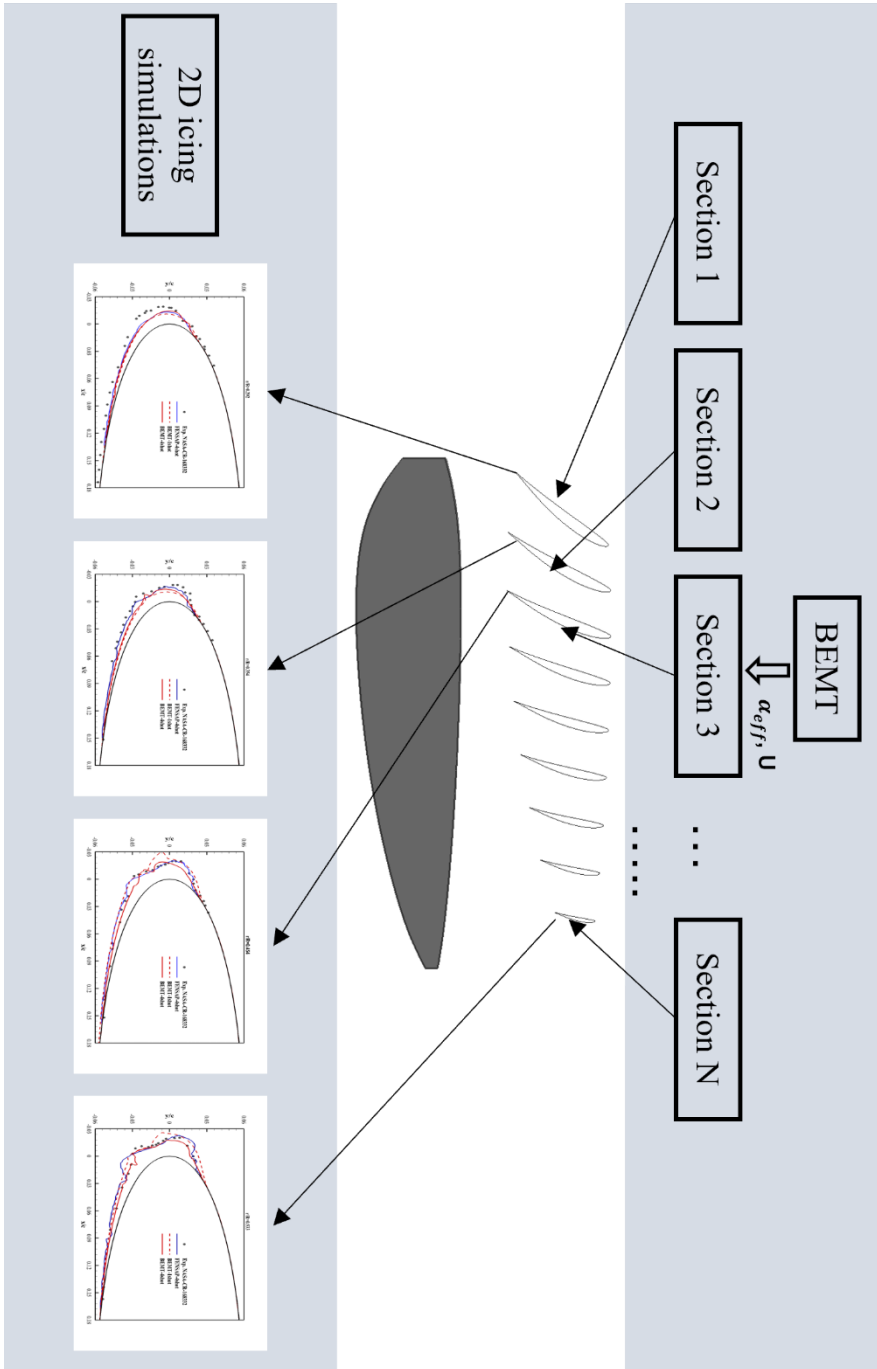

Fig. 4 Structure of the BEMT based icing solver for propeller

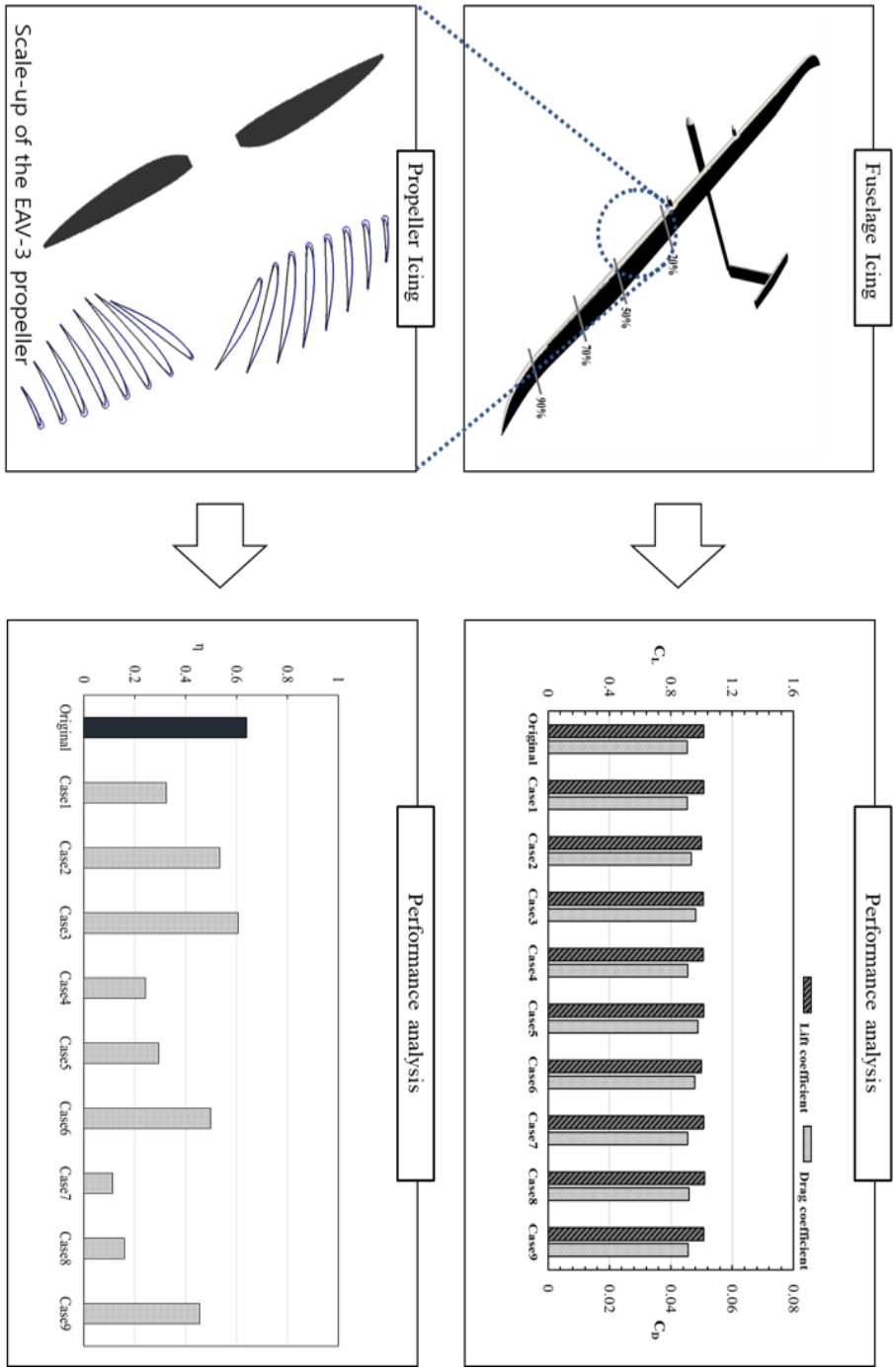

Fig. 5 Individual performance analysis of iced HALE UAV

Next, for the propeller, the Blade Element Momentum Theory (BEMT) approach is used to predict the icing shapes at 2D sections, which are then interpolated to remesh the 3D propeller grid. The newly generated propeller grid is subjected to performance analysis using the Multiple Reference Frame (MRF) method. Finally, propeller's efficiency is calculated to assess its performance using the following equation.

$$\eta = \frac{C_P \cdot J}{C_P} \tag{5}$$

2.4. Determination of operation limit

In this stage, the first step involves calculating the amount of energy required for operation. To determine the energy quantity, the forces acting on the aircraft are computed using the following equations, which then yield the necessary thrust for aircraft operation.

$$\mathrm{D(t)} = C_{D_0}(1 + \Delta C_D \cdot \mathrm{t}/t_{ice}) \cdot \frac{1}{2}\rho(\mathrm{t})U(t)^2\mathrm{A} \tag{6}$$

$$L(\mathrm{t}) = C_{L_0}(1 + \Delta C_L \cdot \mathrm{t}/t_{ice}) \cdot \frac{1}{2}\rho(\mathrm{t})U(t)^2\mathrm{A} \tag{7}$$

$$W(\mathrm{t}) = \mathrm{MTOW}(1 + \Delta\mathrm{M} \cdot \mathrm{t}/t_{ice}) \cdot \mathrm{g} \tag{8}$$

$$\mathrm{T(t)} = \mathrm{L(t)} \cdot \sin(\gamma) + \mathrm{D(t)} \cdot \cos(\gamma) \tag{9}$$

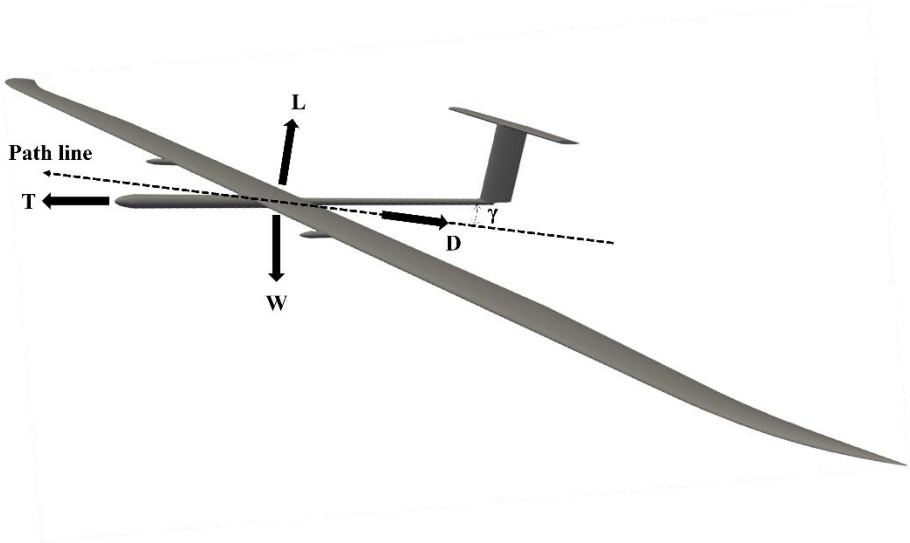

Fig. 6 Forces acting on the fuselage

Utilizing this thrust, along with the velocity and efficiency of the propeller (η_{tot}) used for propulsion, the power or rate of work required for operation is computed using the following equation.

$$\mathrm{P(t)} = \mathrm{T(t)} \cdot \mathrm{V(t)}/\eta_{tot}(\mathrm{t}) \tag{10}$$

The magnitude of thrust is influenced by the increased weight due to icing, and the efficiency of the propeller is affected by the altered shape caused by icing. Consequently, when exposed to icing conditions, these values change over time. For this study, it is assumed that these variations occur linearly with time.

Subsequently, the integration of this rate of work over the operational duration yields the amount of energy required to reach the target altitude (W_{req}).

$$W_{req} = \int_0^t P(t)dt \tag{11}$$

Next, the total energy capacity of the batteries installed in the aircraft is utilized to calculate the amount of supplied energy (W_{prov}). Subsequently, the Battery Margin (BM) value is determined using the following equation.

$$BM = \left(1 - \frac{W_{req}}{W_{prov}}\right) \times 100\ (\%) \tag{12}$$

This BM value is used for ultimately establishing the operational limits. For each icing condition, the BM value is computed, and then the Kriging method is employed to contour the BM values for a wide range of icing conditions. If the BM value falls below a certain threshold, it is considered as a mission failure zone.

Chapter 3. Validation of numerical methods

3.1. In-flight icing code validation

The validity of the current numerical method, when applied to 3D aircraft, has been verified by Son [4]. Son conducted an aerodynamic analysis for the HALE aircraft developed by KARI and obtained lift and drag coefficients. To validate the aerodynamic module, Son compared the results obtained using the commercial solver ANSYS FLUENT [9] with the results obtained using the current numerical method.

3.2. BEMT based 2D icing solver validation

The experimental data on propeller icing for validation is insufficient. Therefore, Helicopter Icing Flight Test (HIFT) results obtained by NASA and the Army [10] were used as a substitute. In general, propellers operate at lower Mach numbers region than rotors. Therefore, the ice shape near the root of the rotor in the low Mach number region is used for validation. The rotor blade used in the experiment was a linearly twisted blade with a NACA 0012 airfoil cross-section, with a chord length of 0.5334m and a radius of 7.3152m.

Table 1 Validation conditions for icing on hovering rotor blade

Property	Value
Temperature(℃)	-30
MVD(μm)	15
LWC(g/m^3)	0.2
Radius(m)	7.3152
RPM	324
Time(s)	180

The icing conditions are summarized in Table 3, and the droplet impingement properties are shown in Fig. 7.

The collection efficiency increased along the span direction due to the increase in inflow velocity, as shown in Fig. 7a. The collection efficiency calculated by the present method and the commercial icing solver FENSAP-ICE' s droplet impingement module DROP3D [11] showed good agreement, as shown in Fig. 7b.

The accreted ice shapes are shown in Fig. 8, where the ice shapes calculated by the FENSAP-ICE [11] and experimental data [10] are compared. Since the present method has been shown to match the experimental results well, it can be considered appropriate to use the present method for interpreting the icing on rotating objects.

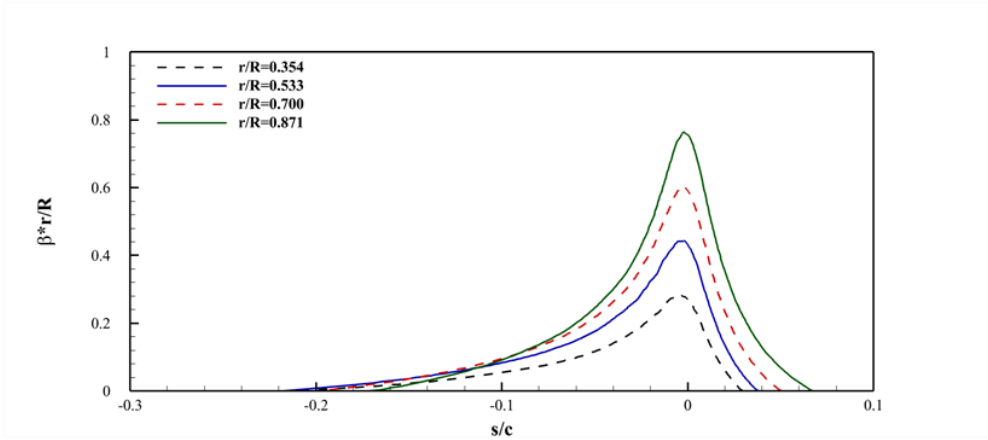

a) Distribution of collection efficiency

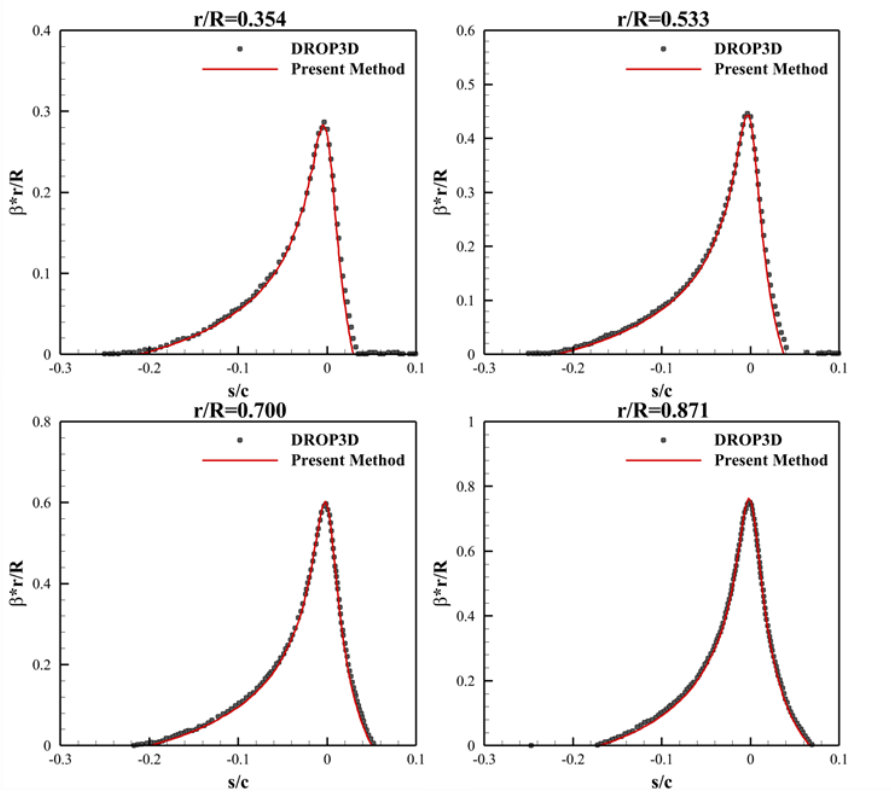

b) Sectional collection efficiency comparison

Fig. 7 Collection efficiency at the different section of the blade

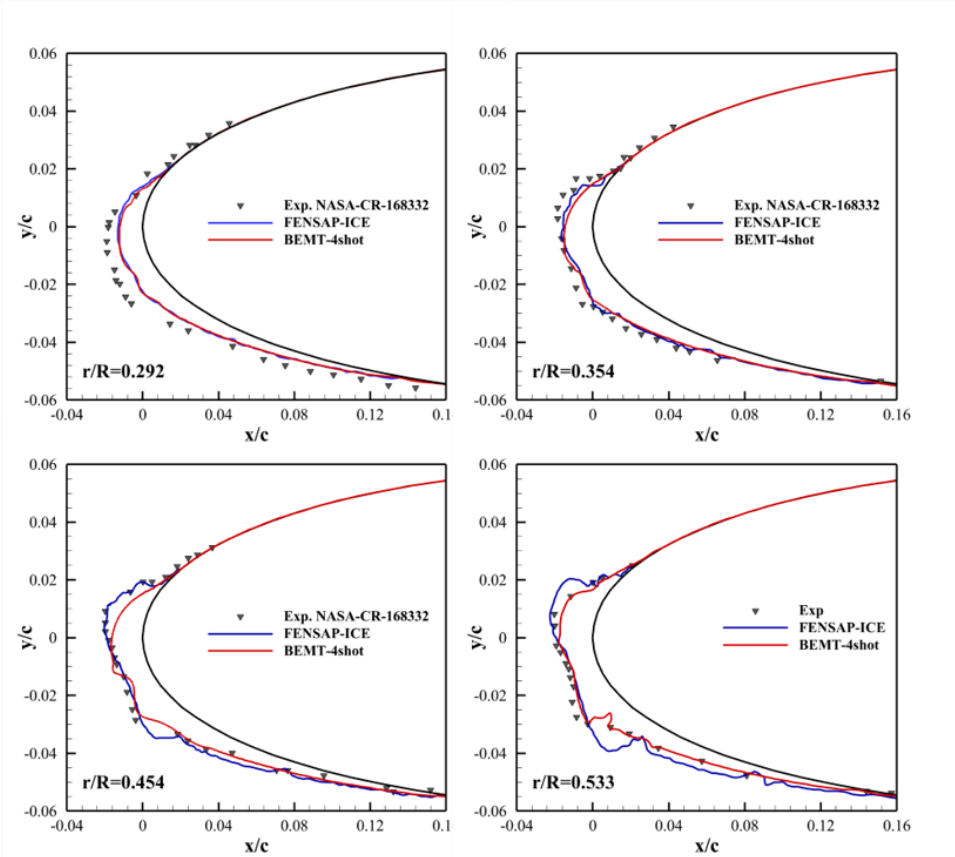

Fig. 8 Sectional ice shape comparison

Chapter 4. Problem definition

To set up the icing simulation environment, the HALE UAV known as EAV-3 [12, 13], developed by the Korea Aerospace Research Institute (KARI), has been selected. This aircraft's specifications are summarized in Table 2.

Table 2 Specification of EAV-3 [12, 13]

Property	Value
MTOW	66kg
Rate of climb	0.75m/s
Cruise speed(V_{cr})	7.8m/s
RPM	925
W_{prov}	37,440,000J

The icing conditions are determined following the regulations specified in the Federal Aviation Regulations (FAR) Appendix C [14]. This regulation outlines the correlations between parameters affecting icing, such as Liquid Water Content (LWC), Median Volume Diameter (MVD), and temperature values. The assumption is made that the aircraft encounters supercooled clouds, and thus, the LWC, MVD, and temperature values at nine different points during these encounters are used for the simulation as shown in Fig. 9 and Table

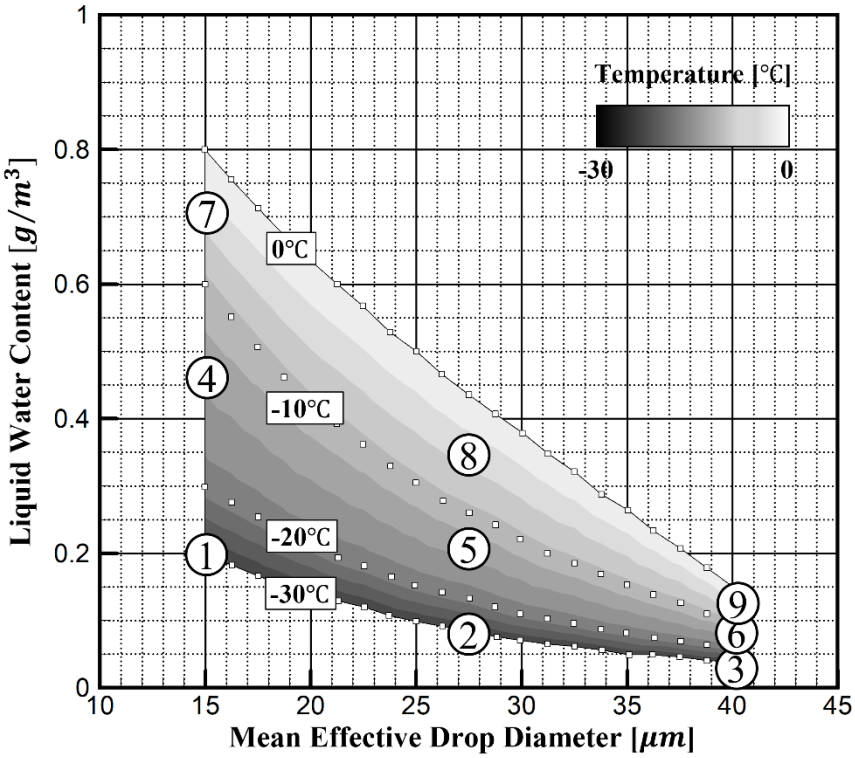

Fig. 9 Icing conditions based on FAR Appendix C

Table 3 Properties of 9 selected icing conditions

Case	LWC(g/m^3)	T(℃)	MVD(μm)
1	0.2	-30	15
2	0.083	-30	27.5
3	0.04	-30	40
4	0.456	-14.25	15
5	0.21	-14.25	27.5
6	0.08	-14.25	40
7	0.77	-1.4	15
8	0.41	-1.4	27.5
9	0.144	-1.4	40

3.

The next consideration is the icing exposure time. This will also be determined by adhering to FAR Appendix C and the mission profile of the HALE UAV as shown in Fig. 10

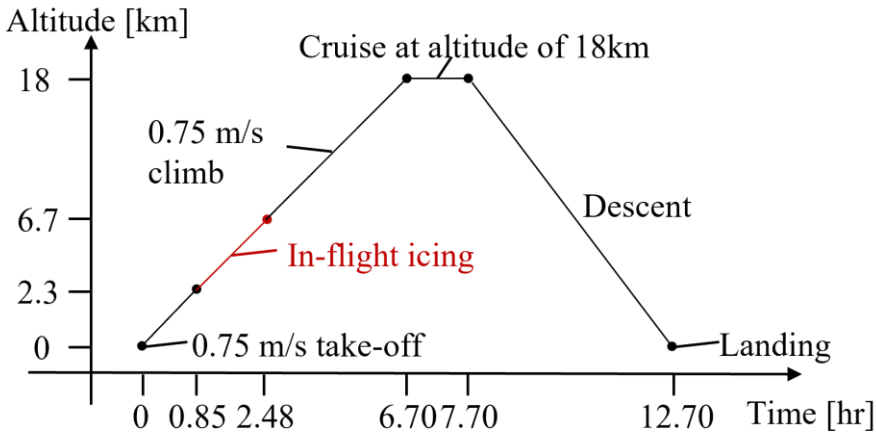

Fig. 10 Mission profile of EAV-3 [12, 13]

Icing occurs when the air temperature is below 0 degrees Celsius, and therefore, the minimum altitude for icing conditions has been set at 2.3 km, which is the altitude where the standard atmospheric temperature reaches 0 degrees Celsius. Furthermore, the maximum altitude for icing conditions has been set at 6.7 km, considering the highest height of stratus clouds assumed to be encountered by the HALE UAV. Given that the aircraft will be exposed to icing conditions between 2.3 km and 6.7 km while maintaining a constant climb rate of 0.75 m/s, the total icing exposure time has been determined to be approximately 1.63 hours.

Chapter 5. Results & Discussions

5.1. Computational domain and boundary condition

The first is the computational domain and boundary conditions utilized in the simulation. The aircraft model used in the simulation is EAV-3, and the boundary condition employed is shown in the Table 4 and Fig. 11.

Table 4 Boundary conditions for icing analysis

Boundary	Type
Inlet	InletOutlet
Outlet	InletOutlet
Side	ZeroGradient
EAV-3 model	No-Slip wall condition

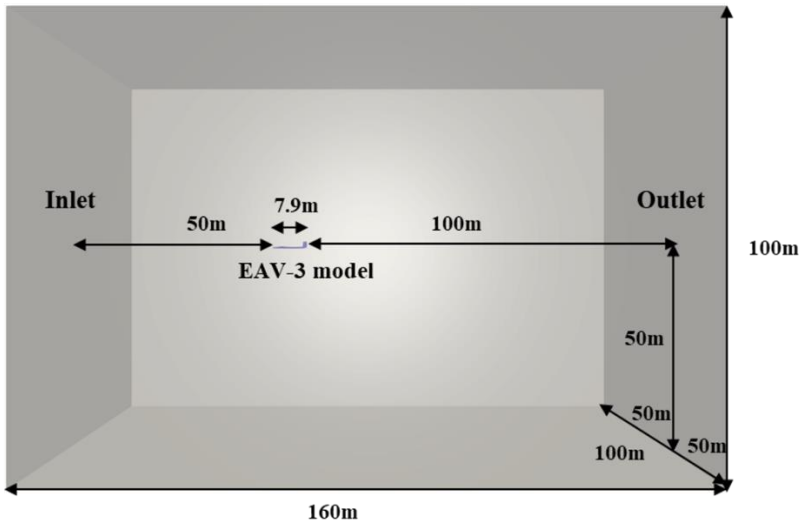

Fig. 11 Boundary condition of the computational grid

For both the inlet and outlet regions of the computational domain, the inletOutlet boundary condition was applied. On the side

boundaries, the zeroGradient boundary condition was used. As for the aircraft model itself, a non-slip wall condition was employed to simulate the interaction with the surrounding fluid flow.

The surface mesh of the grid and cross-section of the grid used in the simulation is depicted in the Fig. 12 and 13. The surface grid consists of 420,000 unstructured cells, while the volume grid consists of 280 million cells with 30 layers of prisms generated using a 1.2 growth rate.

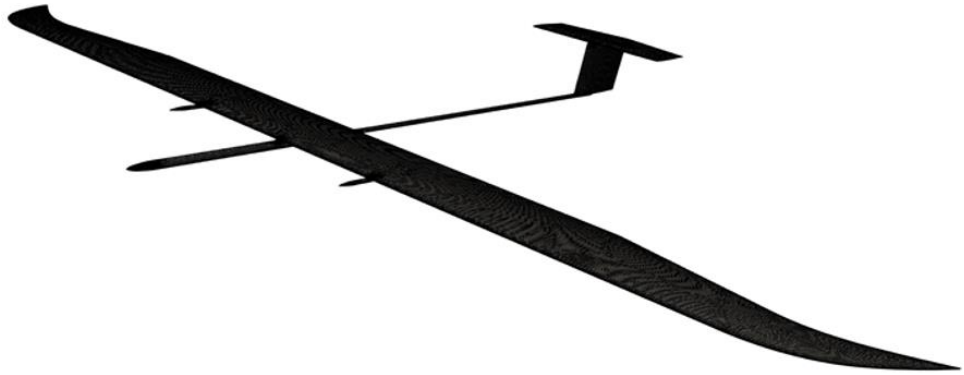

a) Perspective view

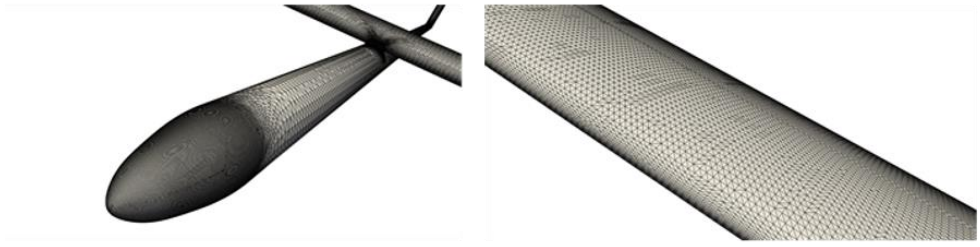

b) Close-up view of head(left) and wing(right)

Fig. 12 Surface mesh of the computational grid

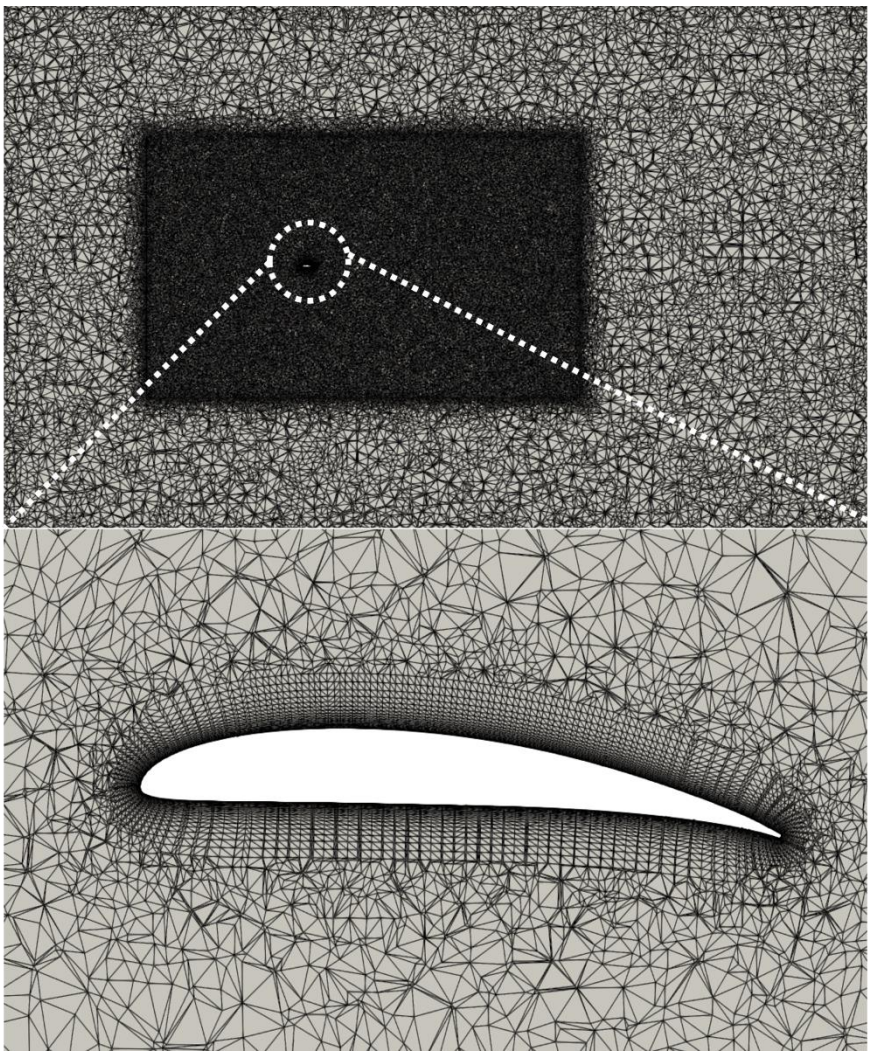

Fig. 13 Slice of the computational grid

5.2. Ice shape prediction and analysis

5.2.1 Icing results of wing & fuselage

Firstly, the graph presented in Fig.14 illustrates the mass growth rate caused by icing. It is evident that all cases exhibit mass growth rates below 5%. This is attributed to the HALE UAV possessing low cruising speeds and long chord lengths, resulting in a low inertia parameter and reduced ice accretion. Moreover, the

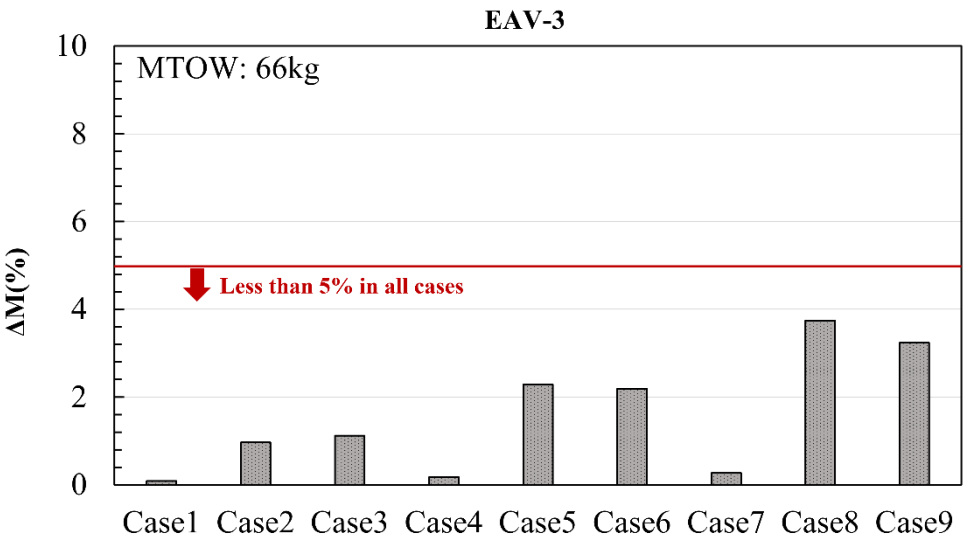

Fig. 14 Comparison of mass increment according to icing condition

Fig. 15 represents the ice accretion as a function of arclength along the mid-section of the aircraft's wing. As the Median Volume Diameter (MVD) decreases, the ice accretion diminishes. Notably, when the MVD is 15 micrometers, the ice accretion tends to converge to zero, indicating minimal impingement of liquid water on the wing's surface.

However, when comparing the graphs of mass growth rates, it is observed that even in cases 1, 4, and 7 with an MVD of 15 micrometers, there is still a discernible mass increase due to icing. To understand the underlying reasons for this, a comprehensive analysis of the ice accretion over the entire aircraft was conducted, as depicted in the Fig. 16.

Notably, while the magnified wing area in the figure exhibits a

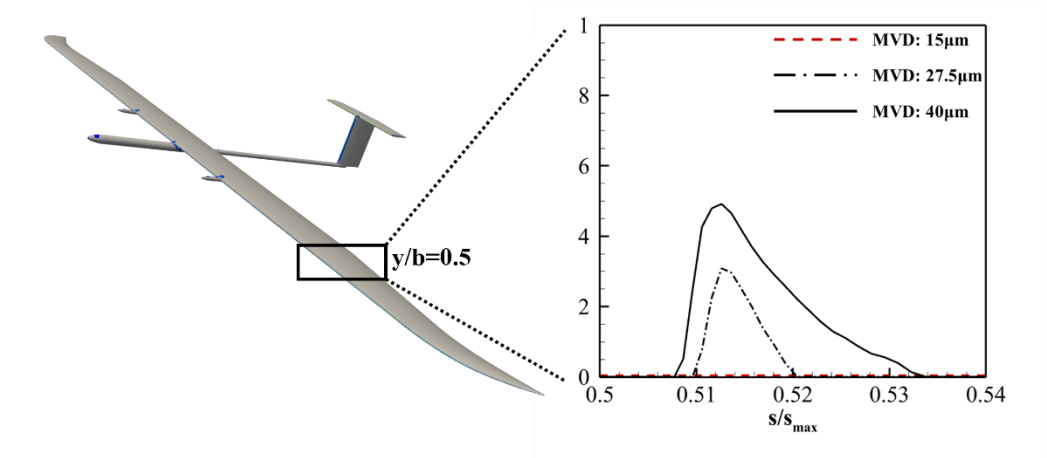

Fig. 15 Collection efficiency contour at the mid-section of the wing

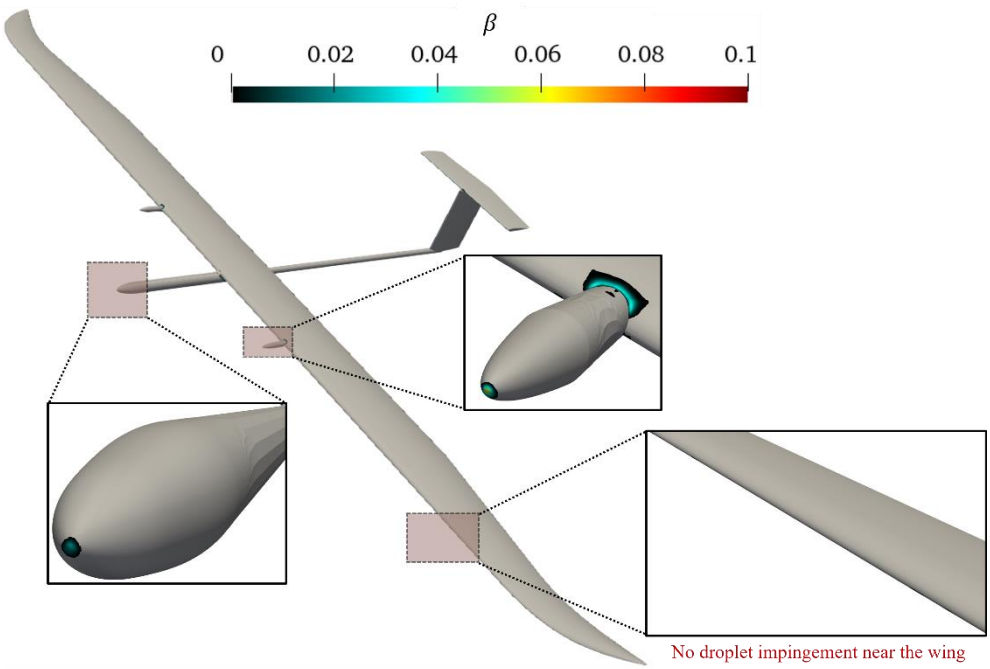

Fig. 16 Collection efficiency contour of cases with low MVD

zero ice accretion value, the head and nacelle sections of the aircraft display non-zero ice accretion values. This discrepancy suggests that although the wing experiences minimal ice formation due to a

lack of liquid water impingement in cases with the lowest MVD values, other regions of the aircraft encounter liquid water impingement, leading to ice formation and a slight increase in mass.

The following section focuses on the verification of icing shapes and the resulting performance variations. The Fig.17 displays the icing shapes at the mid-section of the EAV-3 wing for each case. As noted in the previous ice accretion analysis, the cases with the lowest Median Volume Diameter (MVD) values (Case 1, 4, and 7) indicate ice accretion rates converging to zero, rendering the icing shapes indiscernible in this Fig. 17. Consequently, they have been omitted from the illustration.

Furthermore, consistent with the findings in the analysis of mass growth rates, all cases exhibit negligible changes in icing thickness. The limited ice accretion on the surface restricts the amount of liquid water adhering to the wing, resulting in minimal variations in icing thickness. Notably, in no case does the icing thickness exceed 1% of the chord length, signifying that the observed shape alterations are minimal.

As a result of the extremely limited shape variations caused by icing, it can be inferred that the aerodynamic performance parameters, specifically the lift coefficient and drag coefficient, exhibit almost no differences across all cases as shown in Fig. 18.

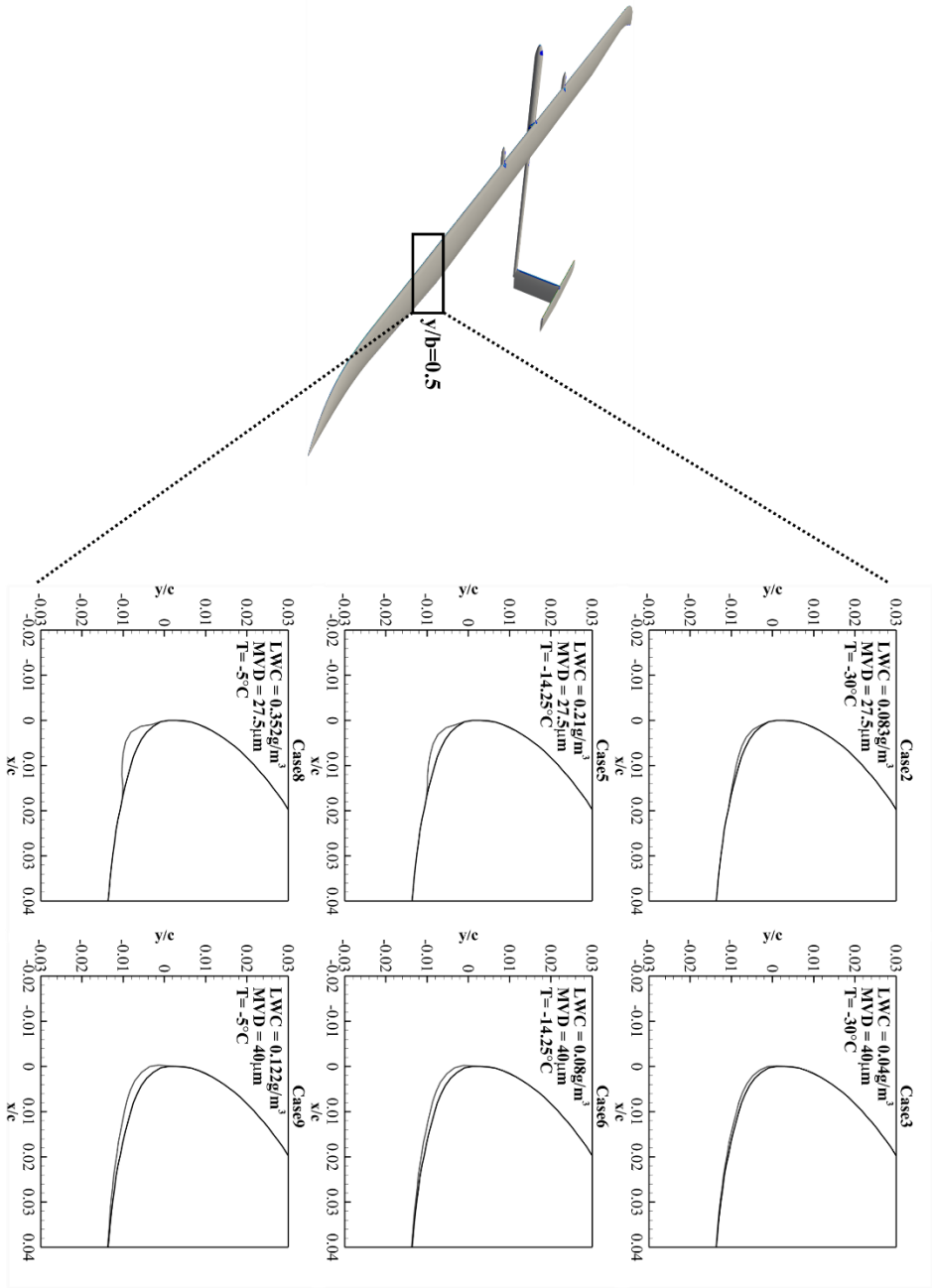

Fig. 17 Ice shapes at the mid-section of the wing

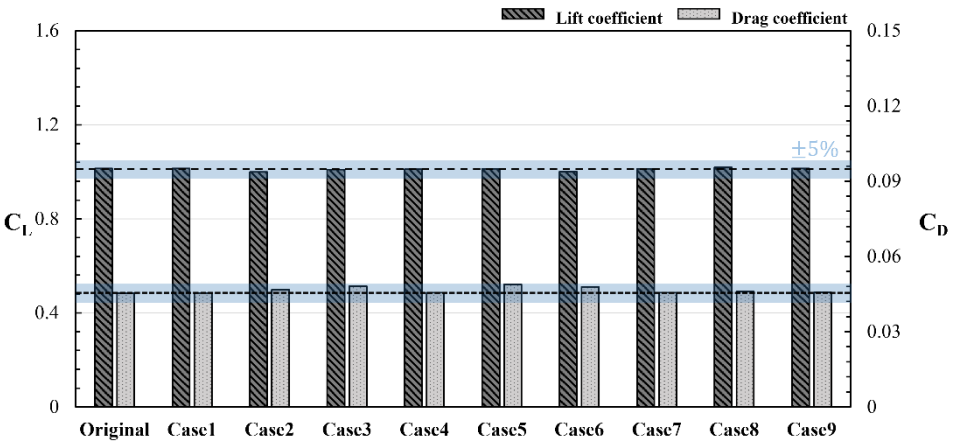

Fig. 18 Lift and drag coefficient in 9 icing conditions

5.2.2 Icing results of propeller

Fig. 19 presents an analysis of the variations in icing shapes and propeller performance at its center section under constant temperature conditions, considering different values of LWC and MVD. Notably, the propeller, characterized by its short chord length and considerably higher velocity compared to the fuselage or wings, exhibits a notably pronounced formation of icing shapes.

Contrary to the fuselage and wing sections where an MVD of 15 micrometers resulted in minimal ice formation, the propeller demonstrates a contrasting behavior. Specifically, lower MVD values in the propeller region correspond to a substantial increase in LWC, leading to a concentration of icing towards the leading edge and significant ice accretion.

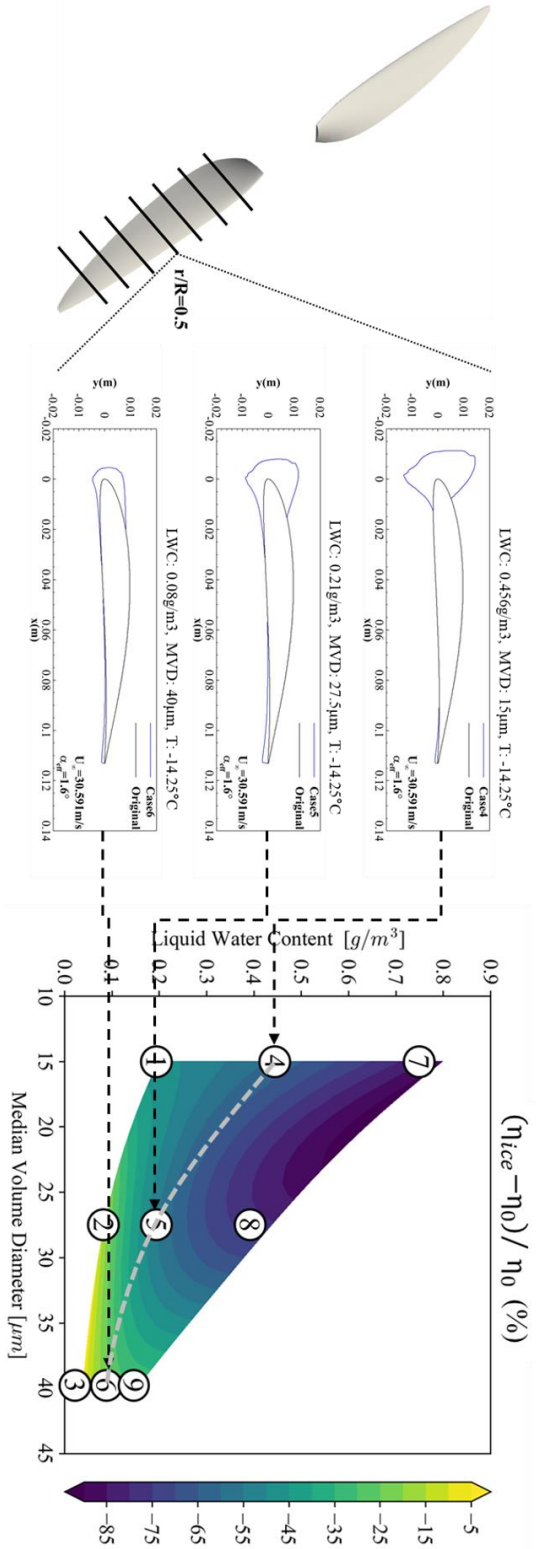

Fig. 19 Comparison of ice shapes and contour of the efficiency of the propeller

The substantial alterations in the propeller's icing shapes, particularly evident when exposed to lower MVD and higher LWC values, consequently, lead to a considerable decrease in propeller efficiency.

5.2.3 Operational limits analysis

Using the previously obtained mass growth rates and changes in aerodynamic performance, the operational limits were determined based on the Battery Margin (BM) values. The results shown in Fig. 20 reveal that the operational range is considerably constrained when compared to the AOPA high-risk region [15], which represents the icing hazard area for transport category aircraft. Additionally, when comparing the outcomes to those obtained without accounting for propeller icing effects as depicted in Fig. 21, it becomes evident that the propeller is significantly influenced by icing, in contrast to the fuselage and wing sections. Consequently, when considering propeller icing, the operational area is notably reduced compared to the case where propeller icing effects were not considered.

In fact, experimental studies on propeller icing have shown that shedding occurs periodically during ice accretion [16, 17]. Therefore, the growth of ice is periodically limited, and the efficiency of the propeller decreases while the ice is accumulated, and when shedding occurs, the efficiency increases again. Therefore, it is expected that

the area where operation is limited will be smaller, considering the shedding effect that actually occurs on the propeller.

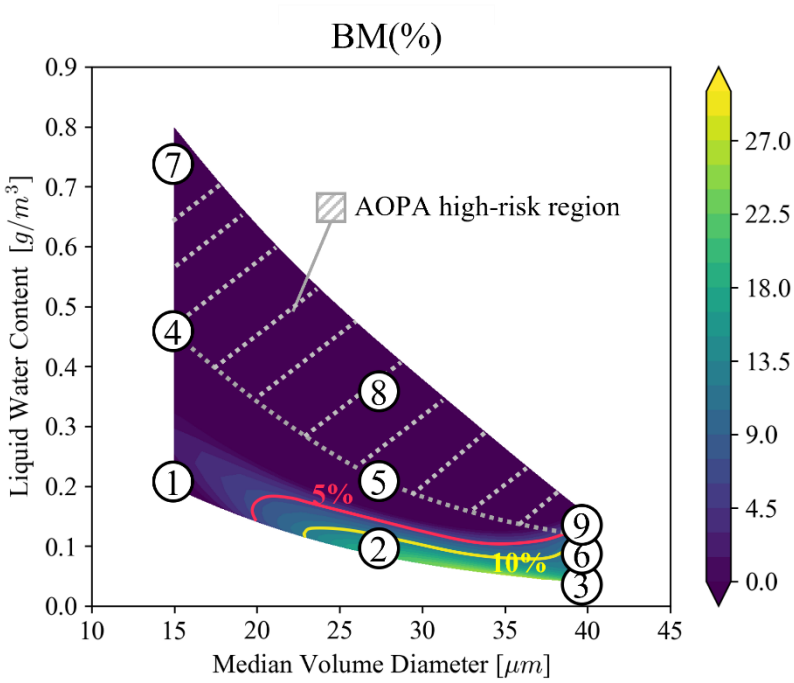

Fig. 20 BM after reaching mission altitude considering propeller icing

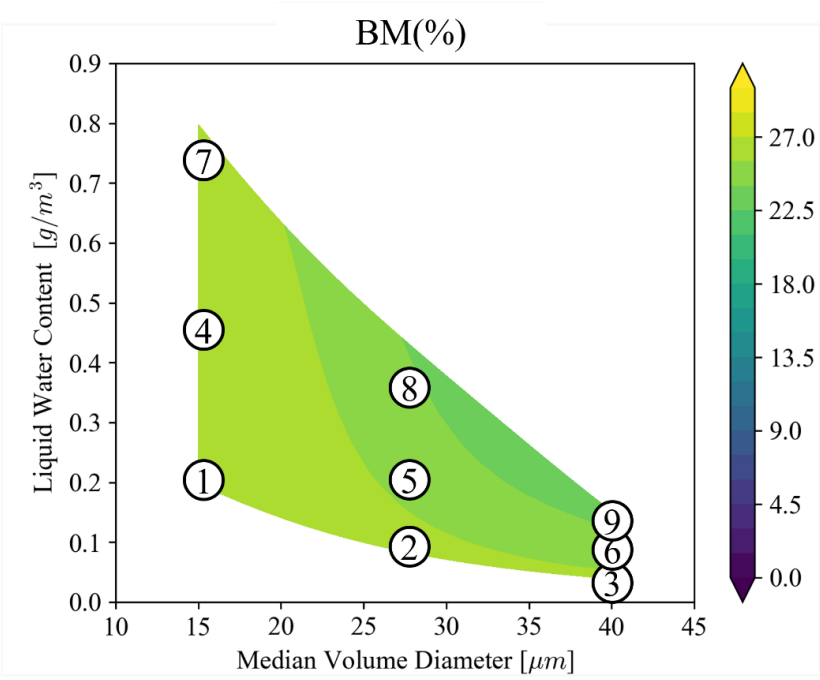

Fig. 21 BM after reaching mission altitude (non-propeller icing)

Chapter 5. Conclusions

In this study, as the first concluding remark, the effects of icing on High-Altitude Long Endurance Unmanned Aerial Vehicles (HALE UAVs) were investigated, considering the icing impact on the propeller. The propeller icing analysis was performed using the Blade Element Momentum Theory (BEMT) approach. Additionally, separate icing simulations were conducted for the wing, fuselage, and propeller sections. The results revealed that the wing and fuselage sections exhibited minor changes in aerodynamic performance, while the propeller experienced a significant decrease in efficiency, up to a maximum of 80%, indicating substantial aerodynamic performance degradation.

Furthermore, through the examination of the effects of propeller icing, it was emphasized that the consideration of propeller icing is crucial for the safe operation of HALE UAVs. When only considering icing effects on the wing and fuselage sections, the results indicated safe operation across all regions. However, once propeller icing effects were taken into account, the safe operational area significantly reduced, as reflected in the values presented below.

As a follow-up to this study, future research will focus on more accurate simulations, considering the interference effects between the wing and propeller. Additionally, the investigation will expand to

include the shedding effects of ice on the propeller, aiming to further enhance the overall accuracy of the analyses.

Bibliography

[1] Vogel, Gerard N. "Icing Considerations for HALE (High Altitude, Long Endurance) Aircraft." *Naval Environmental Prediction Research Facility, Rept. NEPRF-TR-88-11, Monterey, CA* (1988).

[2] IYA, S., and D. COOK. "Icing characteristics of a high-altitude long-endurance aircraft wing airfoil." *29th Aerospace Sciences Meeting*. 1991.

[3] Bottyán, Zsolt. "In-flight icing characteristics of unmanned aerial vehicles during special atmospheric condition over the carpathian-basin." *ACTA Geographica Debrecina Landscape and Environment* 7.2 (2014): 74-80.

[4] Son, Chankyu, and Kwanjung Yee. "Procedure for determining operation limits of high-altitude long-endurance aircraft under icing conditions." *Journal of Aircraft* 55.1 (2018): 294-309.

[5] Son, Chankyu, Sejong Oh, and Kwanjung Yee. "Ice accretion on helicopter fuselage considering rotor-wake effects." *Journal of Aircraft* 54.2 (2017): 500-518.

[6] OpenFOAM, https://www.openfoam.org.

[7] Bourgault, Yves, Héloïse Beaugendre, and Wagdi G. Habashi. "Development of a shallow-water icing model in FENSAP-ICE." *Journal of Aircraft* 37.4 (2000): 640-646.

[8] Leishman, Gordon J. *Principles of helicopter aerodynamics with CD extra*. Cambridge university press, 2006.

[9] Nakakita, Kunio, Siva Nadarajah, and Wagdi Habashi. "Toward real-time aero-icing simulation of complete aircraft via FENSAP-ICE." *Journal of Aircraft* 47.1 (2010): 96-109.

[10] Lee, John D., Rorry Harding, and Richard L. Palko. *Documentation of ice shapes on the main rotor of a UH-1H helicopter in hover*. No. NASA-CR-168332. 1984.

[11] Fouladi, Habibollah. *Computational methods for rotorcraft icing*. McGill University (Canada), 2016.

[12] Hwang, Seung-Jae, et al. "Aerodynamic design of the solar-powered high altitude long endurance (HALE) unmanned aerial vehicle (UAV)." *International Journal of Aeronautical and Space Sciences* 17.1 (2016): 132-138.

[13] Park, Donghun, et al. "Design and performance evaluation of propeller for solar-powered high-altitude long-endurance unmanned aerial vehicle." *International Journal of Aerospace Engineering* 2018 (2018).

[14] Federal Aviation Regulations, “Part 25—Airworthiness Standards: Transport Category Airplanes,” Code of Federal Regulations, U.S. Department of Transportation, Federal Aviation Admin.,Washington, D.C.

[15] “Aircraft Icing,” No. 1, Safety Advisor, Aircraft Owners and Pilots Assoc. Air Safety Foundation, Frederick, MD, 2002, http://www.asf.org [retrieved 01 Sept. 2017].

[16] Anthony, Julian, and Wagdi G. Habashi. "Helicopter rotor ice shedding and trajectory analyses in forward flight." *Journal of Aircraft* 58.5 (2021): 1051-1067.

[17] Müller, Nicolas C., and Richard Hann. "UAV icing: A performance model for a UAV propeller in icing conditions." *AIAA AVIATION 2022 Forum*. 2022.

[17] “Aircraft Icing,” No. 1, Safety Advisor, Aircraft Owners and Pilots Assoc. Air Safety Foundation, Frederick, MD, 2002, http://www.asf.org [retrieved 01 Sept. 2017].

Abstract

프로펠러 결빙을 고려한 고고도 장기 체공 무인기의 운용 한계 결정

Jimin Park
Aerospace Engineering
The Graduate School
Seoul National University

고고도 장기체공 무인기(HALE UAV)는 방송 서비스 제공, 실시간 재난 감시, 정찰 등 다양한 임무를 수행할 수 있기에 세계의 몇몇 연구기관과 제조사들에서 연구, 개발이 되고 있다. 하지만 결빙 조건에서 고고도 장기체공 항공기 운항 시 상승과 하강 비행 과정에서 결빙이 발생하면, 디자인 특성상 제빙 장치를 설치가 힘들기 때문에 결빙에 의한 피해가 발생할 수 있다.

따라서 본 연구에서는 항공기가 마주칠 수 있는 결빙 환경들을 선정하여, 동체, 날개, 그리고 프로펠러에서의 결빙을 시뮬레이션한 후, 바뀐 형상에 대한 성능 분석을 통해 운용에 필요한 총 에너지의 양을 계산하여 항공기의 운용한계 영역을 결정하는 방법을 제시하였다. 이 과정에서 프로펠러 결빙을 2차원 해석 방법(BEMT)을 이용하고, 프로펠러와 동체 & 날개 부분의 개별적인 결빙 해석을 통해 계산 효율성을 높였다. 결과는 동체 & 날개 부분에 발생하는 결빙 형상 및 성능 변화 분석, 프로펠러에 발생하는 결빙 형상 및 성능 변화 분석,

결빙 환경에서의 성능 제한 구역 3가지의 파라미터로 나타냈으며, 프로펠러의 결빙이 고고도 장기체공 무인기의 운용한계에 큰 영향을 끼친다는 것을 확인하였다.

주용어: 고고도 장기체공 무인기, 결빙, 프로펠러, BEMT

학번: 2021-27606